An Analytic Scaling Law for the Depositional Growth of Snow in Thin Mixed-Phase Layer Clouds

VINCENT E. LARSON

University of Wisconsin—Milwaukee, Milwaukee, Wisconsin

ADAM J. SMITH

School of Meteorology, University of Oklahoma, Norman, Oklahoma

(Manuscript received 2 December 2008, in final form 26 February 2009)

ABSTRACT

In various practical problems, such as assessing the threat of aircraft icing or calculating radiative transfer, it is important to know whether mixed-phase clouds contain significant liquid water content. Some mixed-phase clouds remain predominantly liquid for an extended time, whereas others glaciate quickly.

The glaciation rate of mixed-phase layer clouds is thought to depend on various factors, including number concentration of snow crystals, terminal velocity of snow crystals, and crystal habit type. This paper attempts to quantify some of these factors by deriving scaling laws (i.e., power laws) for the mixing ratio and sedimentation flux of snow at cloud base. The scaling laws are derived from the governing equation for snow mixing ratio. They neglect aggregation of snow crystals and accretion of supercooled liquid by snow crystals. The scaling laws permit arbitrary exponents and prefactors of the mass–diameter and fall speed–diameter power laws, allowing flexibility in crystal habit properties.

The scaling laws are tested using idealized large-eddy simulation (LES) of three thin, midlevel layer clouds. The scaling laws agree adequately with the LES over one order of magnitude for snow flux and over two orders of magnitude for snow mixing ratio. They indicate, for instance, that in the present LES, cloud-base snow flux and snow mixing ratio increase faster than linearly with increasing cloud thickness and supersaturation with respect to ice.

By varying the exponents and prefactors of the scaling laws, one may explore the sensitivity of glaciation rate to habit type. The relationship is complex, but, for the cloud cases examined, dendrites tend to glaciate cloud more rapidly than plates.

1. Introduction

There are several reasons that one may wish to know the fraction of liquid water in thin, mixed-phase layer clouds.

One is aircraft icing. Between 1975 and 1988, there were 803 aviation accidents in the continental United States in which icing was a cause or a factor (Bragg et al. 1998). Cober et al. (2001) discuss several well-documented cases of severe icing suffered by research aircraft and also mention the crash of an ATR-72 commuter aircraft near Roselawn, Indiana, in 1994. Icing is particularly hazardous for small aircraft such as unmanned aerial vehicles (UAVs), which often do not have deicing equipment (Haulman 2003).

Furthermore, the amount of liquid water in mixed-phase clouds also influences radiative transfer. Increased liquid water leads to increased shortwave albedo and cloud-top longwave cooling (Sun and Shine 1994). The radiative properties, in turn, affect climate change simulations (Ackerman et al. 2004), generation of cloud-scale turbulence (Marsham et al. 2006), and satellite retrievals of cloud-top temperature (Niu et al. 2008).

Calculating liquid water amounts in mixed-phase clouds requires understanding what processes generate or deplete supercooled liquid water. A key factor is the glaciation rate, that is, the rate at which the average liquid water content in a cloud layer is indirectly converted to ice. In this paper, we will only consider conversion

Corresponding author address: Vincent Larson, Department of Mathematical Sciences, University of Wisconsin—Milwaukee, P.O. Box 413, Milwaukee, WI 53201–0413.
E-mail: vlarson@uwm.edu

DOI: 10.1175/2009JAS3021.1

of liquid to ice via deposition, that is, the Wegener–Bergeron–Findeisen process (Wegener 1911; Bergeron 1935; Findeisen 1938). Furthermore, ''glaciation rate'' will refer to the *net* time rate of change of the ratio of snow to liquid *throughout* a mixed-phase layer. For instance, if a snow crystal forms, grows, and falls out of the mixed-phase cloud base, and any liquid depleted by the crystal is regenerated, then there is no (net) glaciation, as we define it here. [By ''snow,'' we do not mean aggregates, but rather large ice particles of any sort, as distinct from (smaller) cloud ice particles.]

Some mixed-phase clouds have been observed to glaciate within several hours (Hobbs and Rangno 1985), whereas other mixed-phase layers have been observed to persist for days (Pinto 1998; Harrington et al. 1999; Morrison et al. 2005). Why do some mixed-phase clouds glaciate rapidly and others slowly?

If the liquid in a mixed-phase cloud is to persist, the generation rate of liquid must balance or exceed its depletion rate (Rauber and Tokay 1991). Liquid is generated by cloud-top radiative cooling, turbulent transport of moisture, and ascent (Larson et al. 2001, 2006; Smith et al. 2009). In fact, liquid may be regenerated in an entirely glaciated cloud if the updraft velocities are large enough to produce supersaturation with respect to liquid (Rauber and Tokay 1991; Korolev and Field 2008). Liquid is depleted by large-scale descent, radiative heating, turbulent entrainment of dry air, and growth of snow (Larson et al. 2001, 2006; Smith et al. 2009).

Despite the importance of all these processes, this paper will focus solely on understanding the depositional growth rate of snow in thin mixed-phase layer clouds that are statistically homogeneous in the horizontal. What affects the depositional growth of snow and the associated Wegener–Bergeron–Findeisen depletion of liquid? A conceptual sketch may be described as follows. If a snow crystal grows sufficiently large, it falls downward, eventually exiting the mixed-phase cloud base. The mass of liquid removed from the mixed-phase layer depends on crystal size at cloud base. The size depends partly on growth rate and partly on fall speed: if the crystal falls faster, it has less time to accumulate mass before exiting cloud base. The overall glaciation rate depends also on the number concentration of snow crystals, N_S, which in turn depends on the ice nucleation rate. If N_S is greater, then the collective surface area of snow crystals is greater, and hence the collective growth rate is larger. The aforementioned physics has been insightfully discussed and simulated by Harrington et al. (1999). A goal of this paper is to further quantify the strength of these effects by incorporating them into simple explicit formulas.

More specifically, the formulas that we develop are analytic scaling laws for three quantities at cloud base: snow mixing ratio r_S, snow fall speed (i.e., terminal velocity) w_S, and sedimentation flux of snow $w_S r_S$. A scaling law is a power-law relationship between two or more variables. It is distinct from similarity theory, which relates two or more nondimensional parameters but not necessarily by a power-law functional form. These scaling laws are derived by solving a simplified form of the budget equation for r_S that retains the sedimentation and depositional growth terms but ignores all others. The scaling laws for r_S and $w_S r_S$ are tested using large-eddy simulation (LES) of three altostratocumulus (ASc) clouds.[1] Our intent in deriving the scaling laws is not to develop a parameterization that can be implemented in a large-scale host model but, rather, to enhance and quantify our conceptual understanding of what factors affect glaciation rate.

An outline of this paper is as follows: We derive the scaling laws in section 2. To test these scaling laws, we produce benchmark simulations of three cloud cases, designated Nov 11, Oct 14, and Nov 02, described in section 3. The large-eddy model that we use is described in section 4. We compare and overplot the scaling laws and LES output in section 5. We explore the relationship between glaciation rate and habit type in section 6. We conclude in section 7. Table 1 lists major notation used in this paper.

2. Derivation of the scaling laws

The glaciation of mixed-phase clouds depends, in part, on the within-cloud production of snow (which indirectly evaporates liquid) and the removal of this snow from cloud via precipitation. To capture this process, in this section, we derive scaling laws for the snow mixing ratio r_S, snow fall speed w_S, and snow sedimentation flux $w_S r_S$ at the base of a mixed-phase cloud layer.

a. Assumptions of the derivation

This section enumerates the most important assumptions that are required by our derivation.

1) The number concentration of snow crystals, N_S, is diagnosed rather than prognosed. Phrased differently, our derivation is based on a single-moment

[1] Use of ''altostratocumulus'' follows the nomenclature of Larson et al. (2006) and Falk and Larson (2007). They use altostratocumulus to denote overcast altocumulus and reserve ''altocumulus'' to denote partly cloudy altocumulus. This parallels standard nomenclature for boundary layer stratocumulus and cumulus clouds.

TABLE 1. A list of symbols used to derive diagnostic equations (35) and (37). Units and values correspond to those used in our control simulations.

Symbol	Description	Value	Units
A''	Thermodynamic term		$\mathrm{m\ s\ kg^{-1}}$
a''	Constant prefactor in snow fall speed relationship	2.35	
B''	Thermodynamic term		$\mathrm{m\ s\ kg^{-1}}$
b	Fall speed exponent for snow	0.11	
C	Capacitance of snow		m
c_0	Coefficient for r_S		$\mathrm{m}^{3-\beta}$
c_1	Coefficient for PSDEP		$\mathrm{m}^{3-\nu}\ \mathrm{s}^{-1}$
c_2	Coefficient for w_S		$\mathrm{m}^{[-4b/(\beta+1)]+1}\ \mathrm{s}^{-1}$
c_3	Coefficient for PSDEP		$\mathrm{m}^{4(\beta-\nu)/(\beta+1)}\ \mathrm{s}^{-1}$
D_S	Diameter of snow		m
$\overline{D_S}$	Horizontally averaged diameter of snow		m
e_{si}	Saturation vapor pressure for ice		Pa
F'	Constant ventilation factor	2.7	
F_{PSDEP}	Flux of falling snow		$\mathrm{kg\ kg^{-1}\ m\ s^{-1}}$
L	Unit of length in MKS units	1	m
M_S	Mass of a snow crystal		kg
N_S	Number concentration of snow		$\mathrm{m^{-3}}$
N_{0S}	Intercept for snow size distribution	2×10^7	$\mathrm{m^{-4}}$
p	Pressure	52 500 to 58 500	Pa
p_0	Reference pressure	10^5	Pa
PSDEP	Rate of depositional growth of snow		$\mathrm{kg\ m^{-3}\ s^{-1}}$
r_S	Snow mixing ratio		$\mathrm{kg\ kg^{-1}}$
$r_{S,\mathrm{top}}$	Snow mixing ratio at cloud top		$\mathrm{kg\ kg^{-1}}$
R_v	Specific heat of water vapor	461.5	$\mathrm{J\ kg^{-1}\ K^{-1}}$
S_i	Saturation ratio with respect to ice		
t	Time		s
T	Unit of time in MKS units	1	s
w_S	Fall speed of snow		$\mathrm{m\ s^{-1}}$
$\overline{w_S}$	Mass-weighted fall speed of snow		$\mathrm{m\ s^{-1}}$
z	Altitude		m
z_{top}	Altitude at cloud top		m
α	Prefactor for mass–diameter equation	1	
β	Exponent for mass–diameter equation	3	
Γ	Gamma function		
γ	Prefactor in equation for snow capacitance	1	
ν	Exponent in equation for snow capacitance	1	
ρ	Density of air		$\mathrm{kg\ m^{-3}}$
ρ_S	Density of snow	100.0	$\mathrm{kg\ m^{-3}}$
λ_S	Slope of snow size distribution		$\mathrm{m^{-1}}$

microphysics scheme rather than a double-moment scheme. Furthermore, single-moment microphysics is also used in our LES and appears to adequately simulate aircraft observations of our three cases (Smith et al. 2009).

Speaking more physically and specifically, the crucial assumptions are that 1) the snow size distribution is exponential [see Eq. (6) below], 2) the snow intercept parameter N_{0S} is constant with altitude [see Eq. (29) below], and 3) there exist power-law mass–diameter and fall speed–diameter relationships [see Eqs. (8) and (14) below]. These assumptions about number concentration render dubious the application of the scaling laws to cases in which there is strong secondary ice production. However, the scalings can be modified in a straightforward way if the snow number concentration N_S is constant (rather than the snow intercept N_{0S}).

2) Because the microphysics that we use is single moment, we must neglect aggregation. However, aggregation may play a relatively small role in the glaciation of thinner clouds. One of the cloud cases considered (11 November) was not observed to contain many aggregates (Fleishauer et al. 2002), but the other two cases (14 October and 2 November) did contain some aggregates (Carey et al. 2008; Niu et al. 2008). However, we form scaling laws for r_S, not number concentration, and, although the process of aggregation can indirectly change r_S, it directly changes only number concentration.

3) We neglect accretion. Only light riming was shown by aircraft observations of the 11 November cloud by Fleishauer et al. (2002, nor was much riming or graupel observed for the 14 October and 2 November cases (Carey et al. 2008; Niu et al. 2008). Additionally, the LES of Smith et al. (2009) calculated that, for all three cases, accretion was smaller than depositional growth. Furthermore, neglect of accretion is probably necessary so as to yield a simple analytic scaling.
4) We assume that the cloud layer is close to a statistically steady state. By this we do not mean that the cloud remains unchanged with time, but rather that the depositional growth of snow is nearly balanced by fallout. Therefore, we neglect the time tendency of snow. This term is relatively small in the LES of Smith et al. (2009).
5) We neglect turbulent transport of snow. Again, both resolved and subgrid components of this term are relatively small in the LES of thin clouds by Smith et al. (2009), although the term may be larger in thicker clouds with more turbulence.

Although we will test the scaling laws using simulations of thin, mixed-phase, midlevel, midlatitude clouds, the above assumptions do not prohibit the scaling laws from being applied to thin, mixed-phase Arctic clouds at mid or low altitudes.

The neglect of accretion, time tendency, and turbulent transport terms is justified by the simulated budgets of snow mixing ratio presented by Smith et al. (2009). After making these assumptions and the assumption of no aggregation, only two processes remain that contribute to snow growth or decay: deposition and sedimentation. To illustrate this approximate balance of two processes, we shut off accretion and display the resulting budget of snow mixing ratio from the 14 October cloud (Fig. 1). It shows that depositional growth and sedimentation dominate and, hence, are nearly mirror images of each other. Deposition generates the snow mixing ratio in the mixed-phase layer, and sedimentation transports snow from the mixed-phase layer to the bottom of the virga region below, where it sublimates.

b. Derivation

The derivation of the scaling laws is based on the equation for depositional growth of snow. We seek expressions for r_S, w_S, and $w_S r_S$ in terms of "external" quantities such as supersaturation with respect to ice S_i, mixed-phase cloud thickness Δz, and the intercept for snow size distribution N_{0S}. (Although we treat these external quantities as specified forcings, in nature these quantities depend on and interact with the cloud fields themselves.) Our procedure is to (i) write a simplified, steady-state equation for depositional growth of snow; (ii) rewrite this equation in terms of $\overline{D_S}$, the diameter of snow averaged over the size distribution (to do so, we write r_S and w_S in terms of $\overline{D_S}$); (iii) solve for $\overline{D_S}$ in terms of external quantities; and (iv) combine the above expressions to find r_S, w_S, and $w_S r_S$ in terms of external quantities.

1) Write steady-state equation for depositional growth of snow

We construct an equation for depositional growth of snow mixing ratio, r_S, following Rutledge and Hobbs (1983, hereafter RH83):

$$\frac{\partial r_S}{\partial t} = \frac{\partial (w_S r_S)}{\partial z} + \frac{\mathrm{PSDEP}}{\rho} + \frac{\mathrm{PCONV}}{\rho} + \text{turbulent mixing} + \text{accretion}. \quad (1)$$

Here w_S is defined positive downward. Also, ρ is air density, t is time, and z is altitude. The term on the left-hand side is the time tendency term, which is relatively small in our simulations. The first term on the right-hand side is the convergence of the sedimentation flux of snow. The sedimentation term has no explicit negative sign in front of it because w_S is defined to be positive downward. PSDEP is the rate of depositional growth of snow, and PCONV is the rate of conversion from cloud ice (small crystals) to snow (large crystals). Both PSDEP and PCONV have units of mass per volume per time. As stated in the aforementioned assumptions, we neglect turbulent mixing and accretion.

Because we are concerned here only with thin layer clouds of about 1 km or less in thickness, we have used the Boussinesq approximation. In particular, we ignore variations in air density in (1). This is acceptable because the density scale height is $O(10\ \mathrm{km})$, which is much greater than the cloud thickness.

The existence of PCONV is a consequence of the artificial distinction between smaller cloud ice particles and larger snow particles that is commonly made in bulk microphysics schemes. In fact, both cloud ice and snow grow primarily by deposition, so it is reasonable to combine these two terms by use of the following estimate:

$$\mathrm{PCONV} \cong \epsilon\, \mathrm{PSDEP}, \quad (2)$$

where ϵ is a constant. We treat ϵ as a tunable parameter, and set $\epsilon = 0.5$ to best fit our LES. (Because of this tuning, ϵ may in, fact, account for the effects of other terms as well as PCONV.) If we substitute (2) into (1) and neglect the time tendency, turbulent mixing, and

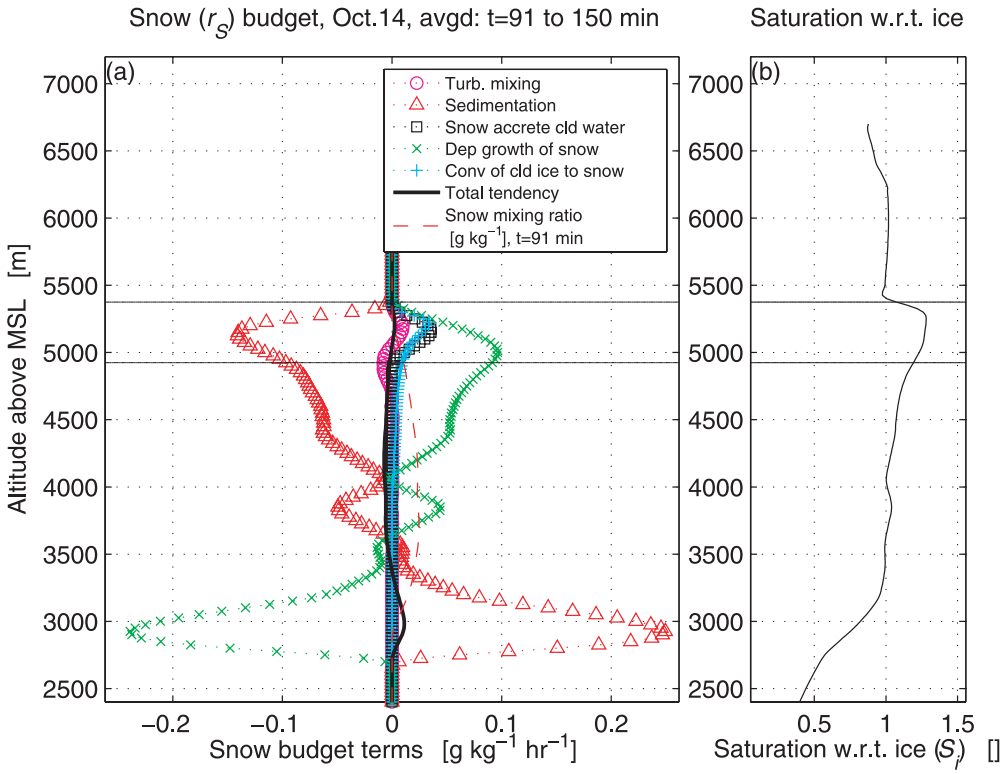

FIG. 1. (a) A budget of snow mixing ratio r_S for the 14 Oct cloud control simulation. The budget is horizontally averaged over a 1-h period from $t = 91$ to 150 min. The overall tendency of the snow mixing ratio is denoted by the thick solid line, and individual model processes are denoted by symbols. For reference, a dashed line indicates the snow mixing ratio profile at $t = 91$ min, and thin horizontal lines indicate the liquid boundaries of the mixed-phase layer. The mixed-phase layer is defined wherever the cloud water mixing ratio (averaged over the horizontal and over times from $t = 91$ to 150 min) exceeds 0.001 g kg^{-1}. (b) A profile of the supersaturation ratio with respect to ice, time averaged from $t = 91$ to 150 min. Horizontal lines indicate the boundaries of the mixed-phase layer, defined as in (a). The budget is dominated by depositional growth of snow (x marks) and sedimentation of snow (triangles), but additional net generators of snow within the mixed-phase layer are the conversion of cloud ice to snow (plus signs) and turbulent mixing (circles). Furthermore, the time tendency (solid black) is also nonnegligible. These data are also plotted in Smith et al. (2009).

accretion terms, we obtain a simple balance between sedimentation and depositional growth of snow:

$$\frac{d(-w_S r_S)}{dz} = (1 + \epsilon)\frac{\text{PSDEP}}{\rho}. \tag{3}$$

The minus sign arises because w_S is defined as positive even though snow falls downward.

We pause now to comment that, given (3), we can already construct an easily interpretable proportionality—namely, if we replace the derivative with respect to z with a finite difference and assume that w_S and r_S are small near cloud top, then

$$\frac{w_S r_S}{\Delta z} \propto \frac{\text{PSDEP}}{\rho}. \tag{4}$$

Here Δz is the thickness of the mixed-phase cloud layer, and w_S and r_S are cloud-base values. Rearranging, we find

$$r_S \propto \frac{\text{PSDEP}}{\rho}\,\tau_S, \tag{5}$$

where $\tau_S \equiv \Delta z / w_S$ is the time scale over which snow falls through the mixed-phase cloud layer. Equation (5) states that r_S is proportional to the depositional growth rate and the time spent by snow crystals in cloud. Although easily interpreted, (5) is incomplete because it does not indicate how PSDEP and τ_S depend on "external" quantities such as S_i and N_{0S}. Furthermore, it will turn out that the simple proportionality $r_S \propto \Delta z$ that one might expect from (4) does not turn out correctly for the Rutledge–Hobbs microphysics discussed below.

To provide a more complete scaling law, we solve Eq. (3) via the following steps. First, we write w_S, r_S, and PSDEP in terms of $\overline{D_S}$; then substitute $w_S(\overline{D_S})$, $r_S(\overline{D_S})$,

and PSDEP ($\overline{D_S}$) into (3) and integrate in z to find $\overline{D_S}(z)$. Finally, we substitute $\overline{D_S}(z)$ into $w_S(\overline{D_S}), r_S(\overline{D_S})$, and PSDEP ($\overline{D_S}$) in order to find $w_S(z)$, $r_S(z)$, and PSDEP(z).

2) WRITE STEADY-STATE SNOW BALANCE [EQ. (3)] IN TERMS OF $\overline{D_S}$

This part of our derivation will generalize RH83 to allow arbitrary power-law mass–diameter and capacitance formulas.

(i) Write r_S and w_S in terms of $\overline{D_S}$

Following Eq. (2) of RH83, we assume an exponential size distribution for snow crystal diameter D_S:

$$dN_S = N_{0S} \exp(-\lambda_S D_S)\, dD_S. \tag{6}$$

Here N_{0S} and λ_S are the intercept and slope of the snow size distribution. We may relate r_S to the size distribution via the formula

$$r_S = \frac{1}{\rho}\int_0^\infty N_{0S} \exp(-\lambda_S D_S) M_S\, dD_S \tag{7}$$

in which M_S is the mass of an individual snow crystal.

We allow for an arbitrary power-law mass–diameter relationship:

$$M_S = \alpha L^3 \frac{\pi}{6}\rho_S \left(\frac{D_S}{L}\right)^\beta. \tag{8}$$

Here α and β are dimensionless constants: values $\alpha = 1$ and $\beta = 3$ correspond to a sphere, which was assumed by RH83. The constant $L = 1$ m is inserted to make the units explicit. Here ρ_S is the density of snow.

Substituting the mass–diameter relationship (8) into (7) and integrating, we find

$$\lambda_S = \left(c_0 \alpha \frac{N_{0S}}{r_S}\right)^{1/(\beta+1)}, \tag{9}$$

where c_0 is a constant, defined as

$$c_0 \equiv \left(\frac{\pi\rho_S}{\rho}\frac{\Gamma(\beta+1)}{6} L^{3-\beta}\right) \tag{10}$$

with units of $L^{3-\beta}$. Equation (9) reduces to RH83's Eq. (3b) if $\alpha = 1$ and $\beta = 3$. Similarly, by integrating over the size distribution, we define

$$\overline{D_S} \equiv \frac{\int_0^\infty N_{0S} \exp(-\lambda_S D_S)\, D_S\, dD_S}{\int_0^\infty N_{0S} \exp(-\lambda_S D_S)\, dD_S} = \frac{1}{\lambda_S} \tag{11}$$

and

$$N_S \equiv \int_0^\infty N_{0S} \exp(-\lambda_S D_S)\, dD_S = \frac{N_{0S}}{\lambda_S} = N_{0S}\overline{D_S}. \tag{12}$$

Here an overbar denotes an average over the size distribution. The relationship $N_S = N_{0S}\overline{D_S}$ is important for understanding the character of the Rutledge–Hobbs scheme. It implies that, for fixed intercept N_{0S}, the snow number concentration N_S is proportional to the diameter of snow crystals $\overline{D_S}$. Therefore, if N_{0S} is kept fixed, then the Rutledge–Hobbs relationship implies that when snow crystals grow larger, they also become more numerous. This is not an unreasonable assumption if both nucleation (Meyers et al. 1992) and growth depend on a common factor, for example, supersaturation with respect to ice. However, it is quite opposite to the process of aggregation in which N_S decreases while $\overline{D_S}$ increases.

Combining Eqs. (9), (11), and (12) implies that

$$r_S = c_0 \alpha N_S \overline{D_S}^\beta. \tag{13}$$

This result is a key step in our derivation. It depends only on the assumptions of an exponential snow size distribution (6) and a power-law mass–diameter relationship (8) and not on any assumption about the deposition, Eq. (3). Snow mixing ratio r_S increases linearly with N_S and increases strongly with $\overline{D_S}$ because $N_S \propto \overline{D_S}$ and $2 \lesssim \beta \lesssim 3$.

The fall speed is given by RH83's Eq. (A4):

$$w_S = a''\left(\frac{L}{T}\right)\left(\frac{D_S}{L}\right)^b \left(\frac{p_0}{p}\right)^{0.4}. \tag{14}$$

Here a'' is dimensionless, and $T = 1$ s is inserted to make the units explicit. Then the velocity averaged over a mass-weighted size distribution is [see Eqs. (A1) and (A5) in RH83]

$$w_S = a''\frac{L}{T}\left(\frac{p_0}{p}\right)^{0.4} \frac{1}{(L\lambda_S)^b}\frac{\Gamma(\beta+b+1)}{\Gamma(\beta+1)}. \tag{15}$$

Substituting (9) for λ_S into (15), we find

$$w_S = c_2 \alpha^{-b/(\beta+1)} a'' N_{0S}^{-b/(\beta+1)} r_S^{b/(\beta+1)}, \tag{16}$$

where

$$c_2 = \frac{L^{(1-b)}}{T}\left(\frac{p_0}{p}\right)^{0.4} \frac{\Gamma(\beta+b+1)}{\Gamma(\beta+1)} c_0^{-b/(\beta+1)}. \tag{17}$$

The quantity c_2 has units of $L^{[-4b/(\beta+1)]+1}T^{-1}$. Substituting the expressions for N_{0S} (12) and r_S (13) into the equation for w_S (16), we find

$$w_S = c_2 c_0^{b/(\beta+1)} a'' \overline{D_S}^{b}. \tag{18}$$

Typically, w_S has a relatively weak dependence on $\overline{D_S}$ because $b < 1$.

As an aside, note that, rearranging (16), we may solve for r_S in terms of w_S and a'':

$$r_S = \alpha N_{0S} \left(\frac{w_S}{a'' c_2} \right)^{(\beta+1)/b}. \tag{19}$$

Equation (19) shows that, if a'' is increased while w_S and N_{0S} are held fixed, then r_S decreases. This is because an increase in a'' while w_S and N_{0S} are held fixed implies a decrease in $\overline{D_S}$ [see Eq. (18)].

(ii) Write PSDEP in terms of $\overline{D_S}$

The depositional growth term, PSDEP, is defined by

$$\frac{\text{PSDEP}}{\rho} = \frac{1}{\rho} \int \left(\frac{\partial M_S}{\partial t} \right)_{\text{Deposition}} dN_S. \tag{20}$$

PSDEP can be derived from the formula [see RH83's Eq. (A16)] for the depositional growth of a single crystal:

$$\left(\frac{\partial M_S}{\partial t} \right)_{\text{Deposition}} = \frac{4\pi C (S_i - 1)}{A'' + B''}. \tag{21}$$

Here $(A'' + B'')$ is a thermodynamic factor that is a function of temperature, thermal conductivity of air, and diffusivity of water vapor in air (RH83; Rogers and Yau 1989).

The quantity C is snow crystal capacitance. How can we interpret it? In (21), regard $(S_i - 1)$ as the driver or forcing, $\partial M_S/\partial t$ as the response, and C as a coefficient that relates the strength of the two. If C is large, snow crystals grow rapidly even in conditions of low supersaturation. We take the capacitance C to be

$$C = \gamma \frac{L}{\pi} \left(\frac{D_S}{L} \right)^{\nu}. \tag{22}$$

Here γ and ν are dimensionless constants. When γ and ν equal 1, the formula reduces to one equivalent to RH83's Eq. (A26). The power-law form (22) is appropriate for platelike or quasi-spherical particles, but not needles or long columns.

To account for the depositional growth of crystals with a range of sizes, we substitute (6), (21), and (22) into (20), integrate over all diameters D_S, and multiply by a constant ventilation factor $F' = 2.7$ that neglects Reynolds number dependence for simplicity and is close to the default values of our LES. Then we find [see RH83's Eq. (A26)]

$$\begin{aligned} \frac{\text{PSDEP}}{\rho} &= \frac{1}{\rho} \frac{4\gamma L (S_i - 1) N_{0S}}{A'' + B''} F' \left(\frac{1}{L\lambda_S} \right)^{\nu} \frac{1}{\lambda_S} \Gamma(\nu + 1) \\ &= c_1 (S_i - 1) N_{0S} \lambda_S^{-\nu-1}, \end{aligned} \tag{23}$$

where

$$c_1 = \frac{1}{\rho} \frac{4\gamma}{A'' + B''} F' L^{-\nu+1} \Gamma(\nu + 1). \tag{24}$$

Here c_1 has units of $L^{3-\nu}T^{-1}$.

To write PSDEP in terms of r_S, we substitute the expression (9) for λ_S into (23):

$$\begin{aligned} \frac{\text{PSDEP}}{\rho} &= c_3 \alpha^{(-\nu-1)/(\beta+1)} (S_i - 1) \\ &\quad \times N_{0S}^{[(\beta-\nu)/(\nu+1)]} r_S^{[(\beta+\nu)/(\beta+1)]}, \end{aligned} \tag{25}$$

where

$$c_3 = c_1 c_0^{(-\nu-1)/(\beta+1)}. \tag{26}$$

Here c_3 has units of $L^{4(\beta-\nu)/(\beta+1)}T^{-1}$.

To write PSDEP in terms of $\overline{D_S}$, we substitute the expressions for r_S (13) and N_{0S} (12) into the equation for PSDEP (25). We find

$$\frac{\text{PSDEP}}{\rho} = c_1 (S_i - 1) N_S \overline{D_S}^{\nu}. \tag{27}$$

3) SOLVE FOR $\overline{D_S}$ IN TERMS OF EXTERNAL QUANTITIES

We have solved for w_S, r_S, and PSDEP in terms of $\overline{D_S}$. Now we solve for $\overline{D_S}$ in terms of the "external" quantities of supersaturation, mixed-phase cloud thickness, and various parameters characterizing ice properties. To do so, we solve the snow budget assuming a steady state (3), which we rewrite here:

$$\frac{d(-w_S r_S)}{dz} = (1 + \epsilon) \frac{\text{PSDEP}}{\rho}. \tag{28}$$

First, we write (28) in terms of the variable $\overline{D_S}$. That is, we substitute into (28) expressions for $r_S(\overline{D_S})$ (13), $w_S(\overline{D_S})$ (18), and PSDEP $(\overline{D_S})$ (27). Next we eliminate $N_S = N_{0S}\overline{D_S}$ [see Eq. (12)], which requires the assumption that N_{0S} is constant with altitude. Then we find that

$$\frac{d}{dz}[(-c_2 c_0^{b/(\beta+1)} a'' \overline{D_S}^{b})(c_0 \alpha \overline{D_S}^{\beta+1})] = (1+\epsilon) c_1 (S_i - 1) \overline{D_S}^{\nu+1}. \tag{29}$$

Taking the derivative of the left-hand side with respect to z, we find

$$-c_2 c_0^{(\beta+b+1)/(\beta+1)} (\beta + b + 1) \alpha a'' \overline{D_S}^{\beta+b} \frac{d\overline{D_S}}{dz} = (1+\epsilon) c_1 (S_i - 1) \overline{D_S}^{\nu+1}. \tag{30}$$

Now we integrate vertically from an altitude within cloud, z, to cloud top, z_{top}:

$$-\int_{\overline{D_S}(z)}^{\overline{D_S}(z_{\text{top}})} \overline{D_S}^{\beta+b-\nu-1} \, d\overline{D_S} = (1+\epsilon) \frac{c_1}{c_2} c_0^{-(\beta+b+1)/(\beta+1)} (\beta + b + 1)^{-1} \alpha^{-1} a''^{-1} \int_z^{z_{\text{top}}} (S_i - 1) \, dz. \tag{31}$$

For simplicity, assume that $\overline{D_S}$ at the top of the layer is negligible. Then the mean snow diameter, $\overline{D_S}$, is given by

$$\overline{D_S}(z) = c_0^{-1/(\beta+1)} \left[(1+\epsilon) \frac{c_3}{c_2} \frac{\beta + b - \nu}{\beta + b + 1} \alpha^{-1} a''^{-1} (\langle S_i \rangle - 1)(z_{\text{top}} - z) \right]^{1/(\beta+b-\nu)}, \tag{32}$$

where angle brackets denote a vertical average from z to z_{top}. In principle, z can represent any altitude within the mixed-phase cloud layer, but in practice we will usually interpret $z_{\text{top}} - z = \Delta z$, the mixed-phase cloud thickness. Writing $\langle S_i \rangle$ as a constant cloud-layer average rather than as a function of z is an approximation, but it is more accurate than simply using the value of S_i at cloud base. From (32), we see that the mean diameter $\overline{D_S}$ has no explicit dependence on N_{0S} or N_S, as expected.

Equation (32) can be more easily interpreted by taking the $(\beta + b - \nu)$th power of (32), rearranging the resulting equation, and multiplying both sides of it by N_S. Then we find

$$w_S r_S \propto \underbrace{a'' \overline{D_S}^{b}}_{\propto w_S} \underbrace{N_S \alpha \overline{D_S}^{\beta}}_{\propto r_S} \propto \underbrace{N_S \overline{D_S}^{\nu} (\langle S_i \rangle - 1)}_{\propto \text{PSDEP}} (z_{\text{top}} - z). \tag{33}$$

Equation (33) resembles the steady-state r_S budget (28) and has the same exponents. This is because (33) is essentially the vertical integral of (28). Therefore, (33) may be interpreted as a steady-state balance between the layer-integrated source, PSDEP$(z_{\text{top}} - z)$, and the sink due to snow flux out the cloud base, $w_S r_S$.

Inspection of (33) can help us interpret the functional dependence of the exponent, $1/(\beta + b - \nu)$, on β, b, and ν in the preceding equation for $\overline{D_S}$ (32). To start, Eq. (33) helps us glean which processes are most deeply involved in this exponent via the origins of the parameters: β from the mass–diameter relationship (8), b from the fall speed–diameter relationship (14), and ν from the capacitance (22). Now regard $[(\langle S_i \rangle - 1)(z_{\text{top}} - z)]$ as the specified forcing and the snow flux at cloud base, $w_S r_S$, as the response. An increase in $[(\langle S_i \rangle - 1)(z_{\text{top}} - z)]$ leads to a linear increase in $w_S r_S$. However, the increase in mean diameter at cloud base, $\overline{D_S}$, depends also on the exponents b and β. The reason is that $w_S r_S$ depends nonlinearly on $\overline{D_S}$. For instance, according to our mass–diameter relationship (8) and its corollary for r_S (13), if β is large and positive, then only a small increase in $\overline{D_S}$ leads to a large increase in r_S. Similarly, according to our fall speed–diameter relationship (14) and its corollary for w_S (18), if b is positive, then an increase in $\overline{D_S}$ leads to an increase in w_S. Therefore, if $(\beta + b)$ is large and positive, then a large increase in $[(\langle S_i \rangle - 1)(z_{\text{top}} - z)]$ may lead to a large increase in $w_S r_S$, but this large increase in $w_S r_S$ requires only a small increase in $\overline{D_S}$. That is, because of the strong dependence of $w_S r_S$ on $\overline{D_S}$, only a small change in $\overline{D_S}$ is needed to balance a large change in $[(\langle S_i \rangle - 1)(z_{\text{top}} - z)]$. In accordance with this physics, $\beta + b$ appears in the denominator of the exponent in (32), $\overline{D_S} \propto [(\langle S_i \rangle - 1)(z_{\text{top}} - z)]^{1/(\beta+b-\nu)}$.

The other factor that affects $\overline{D_S}$ is the capacitance, $C \propto \overline{D_S}^{\nu}$. The capacitance is a shape-dependent factor that governs how effectively a snow crystal can take up ambient vapor. Mathematically, the capacitance is a prefactor that increases $w_S r_S$ for a given value of $[(\langle S_i \rangle - 1)(z_{\text{top}} - z)]$ [recall the comments above Eq. (22)]. If ν is large and positive, then there is a strong positive feedback to changes in $\overline{D_S}$. For instance, an increase in $\overline{D_S}$ increases C, which in turn increases PSDEP, which in turn causes $\overline{D_S}$ to grow. To represent

this positive feedback, ν appears with a minus sign in the denominator of the exponent of (32).

From (32), we see that $\overline{D_S}$ decreases as the fall speed coefficient a'' or mass–diameter coefficient α increases. Specifically, $\overline{D_S} \propto a''^{-1/(\beta-b-\nu)}\alpha^{-1/(\beta-b-\nu)}$. Why does this dependence arise? If a'' increases, then w_S increases, necessitating a decrease in $\overline{D_S}$ to maintain a balance between cloud-base snow flux and depositional growth. More physically, an increase in a'' and hence w_S gives snow crystals less time to grow in the mixed-phase cloud layer, leading to smaller $\overline{D_S}$. The mass–diameter coefficient α enters Eq. (32) the same mathematical way as does a'' and hence has the same exponent.

4) Solve for r_S, w_S, and $w_S r_S$ in terms of external quantities

At this point, to solve for r_S we merely need to substitute into the formula for $r_S = r_S(N_S, \overline{D_S})$ (13) the expressions for $N_S(\overline{D_S})$ (12) and $\overline{D_S}$ (32). (Recall that the equation for $\overline{D_S}$ is derived from a steady-state balance of snow production and sedimentation flux convergence. Therefore, the following equations are consistent with this simple balance.) We find

$$r_S(z) = \left[(1+\epsilon)\frac{c_3}{c_2}\frac{\beta+b-\nu}{\beta+b+1}\right]^{(\beta+1)/(\beta+b-\nu)} N_{0S}\alpha^{(b-\nu-1)/(\beta+b-\nu)}[a''^{-1}(\langle S_i\rangle - 1)(z_{\text{top}} - z)]^{(\beta+1)/(\beta+b-\nu)}. \quad (34)$$

If r_S at cloud top is nonzero, then we can generalize (34) to find

$$r_S(z) = \left[(1+\epsilon)\frac{c_3}{c_2}\frac{\beta+b-\nu}{\beta+b+1}\alpha^{(b-\nu-1)/(\beta+1)}a''^{-1}N_{0S}^{(\beta+b-\nu)/(\beta+1)}(\langle S_i\rangle - 1)(z_{\text{top}} - z) + r_{S,\text{top}}^{(\beta+b-\nu)/(\beta+1)}\right]^{(\beta+1)/(\beta+b-\nu)}. \quad (35)$$

We can also write w_S in terms of external quantities by substituting (34) into (16):

$$w_S(z) = \left[(1+\epsilon)c_3\frac{\beta+b-\nu}{\beta+b+1}\right]^{b/(\beta+b-\nu)} c_2^{(\beta-\nu)/(\beta+b-\nu)}\alpha^{-b/(\beta+b-\nu)}a''^{(\beta-\nu)/(\beta+b-\nu)}[(\langle S_i\rangle - 1)(z_{\text{top}} - z)]^{b/(\beta+b-\nu)}. \quad (36)$$

Finally, we can find the snow flux $w_S r_S$ by multiplying the expressions for w_S (36) and r_S (34):

$$w_S(z)r_S(z) = \left[(1+\epsilon)c_3\frac{\beta+b-\nu}{\beta+b+1}\right]^{(\beta+b+1)/(\beta+b-\nu)} c_2^{(-\nu-1)/(\beta+b-\nu)}N_{0S}\,\alpha^{(-\nu-1)/(\beta+b-\nu)}a''^{(-\nu-1)/(\beta+b-\nu)} \times [(\langle S_i\rangle - 1)(z_{\text{top}} - z)]^{(\beta+b+1)/(\beta+b-\nu)}. \quad (37)$$

The snow flux at cloud base, $w_S r_S$, is a relevant quantity because it is related to the net source of snow within cloud. To derive the relationship, we assume that $r_{S,\text{top}} = 0$ and integrate (3) from cloud base to cloud top. This yields

$$\underbrace{w_S r_S|_{\text{Cloud base}}}_{\text{Cloud base snow flux}} = \underbrace{\int_{\text{Cloud base}}^{\text{Cloud top}} (1+\epsilon)\frac{\text{PSDEP}}{\rho}\,dz}_{\text{In-cloud source of snow}}. \quad (38)$$

As an aside, we note that one could go further and use $w_S r_S|_{\text{Cloud base}}$ to compute a glaciation time scale τ_G. To do so, we write the time tendency of sedimentation as

$$\left(\frac{\partial r_S}{\partial t}\right)_{\text{Sed}} = \frac{\partial(w_S r_S)}{\partial z}. \quad (39)$$

Taking finite differences of (39), we see that the time scale τ_G required for sedimentation, acting alone, to deplete a cloud layer with vertically averaged snow mixing ratio, $\langle r_s\rangle$, would be

$$\tau_G \propto \frac{\langle r_S\rangle \Delta z}{w_S r_S|_{\text{Cloud base}}}. \quad (40)$$

The time scale τ_G differs from the aforementioned time scale τ_S (5) for snow to fall through a cloud layer. The time scale τ_G is of physical interest, but it requires extra assumptions about the vertical average of r_S to compute, and so we leave its analysis for future work.

3. Cloud cases used to test the scaling laws

To test the scalings derived in the previous section, we simulate three mixed-phase layer clouds that were

TABLE 2. Key properties of the Nov 11, Oct 14, and Nov 02 cloud cases. The clouds are similar in many respects but exhibit differences in temperature and, relatedly, snow mixing ratio r_S.

Variable	Nov 11	Oct 14	Nov 02
Initial mixed-phase cloud-top altitude, MSL (m)	5700	5300	4700
Mixed-phase cloud thickness (m)	500	700	400
Mixed-phase cloud-top temperature (°C)	−16	−22	−13
Mean observed r_S (g kg^{-1})	0.02	0.04	0.005
Observed cloud-top cloud water r_c (g kg^{-1})	0.4	0.25	0.15

observed by aircraft (Fleishauer et al. 2002; Carey et al. 2008; Smith et al. 2009). We denote the clouds by the date of observation: 11 November, 14 October, and 2 November. We now describe these cases briefly; for details of the aircraft observations, see Smith et al. (2009).

The Nov 11 cloud was sampled by an aircraft over central Montana on 11 November 1999 during the fifth of the Complex Layered-Cloud Experiments (CLEX-5). Descriptions of the observations and instrumentation are provided in Fleishauer et al. (2002). The Oct 14 and Nov 02 clouds were sampled during the ninth of the Complex Layered-Cloud Experiments (CLEX-9) over Nebraska in 2001. For a description of these cases, see Kankiewicz et al. (2002) and Carey et al. (2008).

The clouds shared some similarities. All three clouds were altostratocumulus clouds (Larson et al. 2006); in other words, they were thin, overcast layer clouds (analogous to low-level stratocumulus clouds), and they resided in the midlevels of the troposphere (thus classifying these layers as alto clouds). In all three cases, peak liquid occurred primarily at cloud top, and ice fell out of the mixed-phase cloud base, forming virga that did not reach the ground.

However, the three clouds also had differences. Several of these differences stemmed from the fact that the Nov 11 cloud was embedded in a descending air mass (Larson et al. 2001), whereas the Oct 14 and Nov 02 clouds were embedded in ascending air (Smith et al. 2009). A few key properties of the three clouds are listed in Table 2. The Oct 14 mixed-phase layer was coldest and thickest, and the Nov 02 mixed-phase layer warmest and thinnest. Therefore, snow particles in the Oct 14 cloud experienced the largest vertically integrated supersaturation with respect to ice. This contributes to the fact that Oct 14 had the greatest r_S, Nov 11 the next greatest, and the Nov 02 cloud the least. The largest liquid water content, however, was measured in the Nov 11 cloud.

We cannot use the observations directly to construct a scaling law because the number of cases is so limited. Instead, we simulate these cases and also perform a suite of sensitivity simulations based on them.

4. LES model description and configuration

We now briefly describe the large-eddy model that we use and the configuration for each case. For details, see Smith et al. (2009).

a. LES dynamical model and microphysics scheme

To perform cloud simulations, we use the Coupled Ocean–Atmosphere Mesoscale Prediction System (COAMPS) LES model (Golaz et al. 2005). This model has been previously used for high-resolution, three-dimensional LES studies of observed midlevel altostratocumulus cases (Larson et al. 2006; Falk and Larson 2007; Smith et al. 2009). A general description of the model is available in Hodur (1997), its application to altostratocumulus simulations is detailed in Larson et al. (2006), and comparisons of model simulations with observations for our three cases are detailed in Smith et al. (2009).

Radiative formulas and the corresponding radiative constants are summarized in Larson et al. (2007). The longwave radiative flux is calculated following Stevens et al. (2005). Shortwave radiation is calculated using the two-stream, single-band model of Shettle and Weinman (1970) and Duynkerke et al. (2004). We also apply large-scale ascent or descent to individual simulations by selecting a constant vertical velocity and using it to vertically advect water vapor, potential temperature, and horizontal winds.

COAMPS-LES uses a single-moment bulk microphysical scheme based on RH83. Detailed information on the microphysical equations and parameter values that we use can be found in Long (2003). The scheme predicts the mixing ratio of five hydrometeor species: cloud water (r_c), rain (r_r), cloud ice (r_i), snow (r_S), and graupel (r_g). In all of our cloud cases, aircraft observations show no evidence of graupel, rain, or drizzle, so we deactivate these processes in our simulations. Because the scheme is single moment, it diagnoses number concentration and hence cannot simulate aggregation. Furthermore, to compare more closely with our scaling law, we deactivate accretion (riming).

In our simulations, we calculate ice particle number concentration, N_i, as the maximum computed by the formulas of Fletcher (1962) and Cooper (1986). At each grid point where microphysics is applied, N_i is calculated from each formula and the largest diagnosed concentration is used. We have tested alternative ice nucleation formulas, such as Meyers et al. (1992) and the individual Fletcher and Cooper formulas. For our cases, the combined Fletcher–Cooper method generates a more accurate snow mixing ratio than either the Fletcher or Cooper formulas alone, or the Meyers formula (Smith et al. 2009).

b. Configuration of COAMPS-LES

All of our simulations share the following settings. The horizontal grid spacing is 75 m × 75 m, and the vertical grid spacing is 25 m. The horizontal domain size is 4125 m × 4125 m. Because the cloud systems are all isolated from the boundary layer, surface and momentum fluxes at the lower model boundary are set to zero. The time step is 1 s, and the total duration of each simulation is 4 h. Simulated results are averaged over the hour following spinup (90–150 min). We choose this hour because during this time, all three clouds exist and closely resemble observations. The Nov 11 cloud water diminishes during this time, but the other two cases are closer to steady state (Smith et al. 2009).

Case-specific settings are listed below.

1) THE NOV 11 CLOUD

The Nov 11 cloud was the subject of a three-dimensional LES simulation study in Larson et al. (2006). In the previous study, a simplified ice parameterization was used to simulate depositional growth of ice. However, we now wish to focus on snow and the factors that affect its growth. Therefore, we use the single-moment Rutledge–Hobbs microphysical scheme described above.

To simulate the virga below cloud, the vertical domain is now increased to 4400 m from the previous study's vertical domain of 2400 m. The model base is now placed at 3000 m MSL. The large-scale descent is set to 3 cm s^{-1}, based on a short-term high-resolution forecast (Larson et al. 2006). To calculate shortwave radiation, the solar zenith angle is set to a constant value since this cloud lasted only briefly before dissipating. Longwave radiative constants are described in Larson et al. (2006).

2) THE OCT 14 CLOUD

Because the Oct 14 cloud was observed at roughly the same latitude and longitude as the Nov 11 cloud, we use the same longwave radiation constants provided in Larson et al. (2006). However, because the Oct 14 cloud lasted longer than the Nov 11 cloud, we allow the solar zenith angle to vary. To calculate the solar zenith angle, we use the methodology of Liou (2002, 45–49).

Both the aircraft observations and the supplemental sounding indicate strong vertical wind shear. In our simulations, we subtract the mean horizontal wind velocity to produce a wind profile relative to cloud motion. For large-scale ascent, a value of 1.4 cm s^{-1} was obtained based on data from the National Centers for Environmental Prediction (NCEP) North American Regional Reanalysis (NARR) at 1200 and 1500 UTC 14 October 2001. The vertical domain is set to 4500 m with the model base located at 2213 m MSL.

3) THE NOV 02 CLOUD

The Nov 02 cloud was sampled in nearly the same geographic location as the Oct 14 case, so the same longwave radiation constants were selected. A varying solar zenith angle is used, as for the Oct 14 case. Finally, for large-scale ascent, we impose from the NCEP NARR a velocity of 0.7 cm s^{-1} based on data obtained from 1200 and 1500 UTC 2 November 2001. For this case, the simulated vertical domain was 3000 m, with model base located at 3097 m MSL.

5. Comparison of analytic scaling laws with LES calculations

We now compare our analytic scaling laws to COAMPS-LES output. Specifically, we test our analytic formulas for the snow mixing ratio r_S at cloud base (35) and snow sedimentation flux $w_S r_S$ at cloud base [i.e. the product of (36) and (35)].

To test the functional forms of the scaling laws, we perform a sensitivity study in which the atmospheric conditions are varied widely. Each sensitivity simulation is based on one of the three aforementioned altostratocumulus clouds, that is, the Nov 11, Oct 14, and Nov 02 clouds. The parameters varied are a'', which affects the fall velocity of snow; N_{0S}, which affects the number of snow particles produced; and the large-scale ascent w_{ls}, which indirectly modifies the saturation mixing ratio. These parameters are varied over wide ranges that are likely to include most of the values for ASc observed in nature. Numerical values for each parameter are listed in Tables 3 and 4. The set of parameter values for each sensitivity simulation is chosen as follows. First, we choose a cloud case. Then we select a single parameter to vary and select its value from Table 3 or 4. We set all other sensitivity parameters to

TABLE 3. Imposed sensitivity values of large-scale vertical velocity (w_{ls}) for each cloud case. Positive values (cm s^{-1}) indicate ascent. In each w_{ls} sensitivity simulation, a single value of ascent or descent is selected, and all other parameters are set to their control values. An asterisk denotes the control setting for each cloud case.

Nov 11 w_{ls}	Oct 14 w_{ls}	Nov 02 w_{ls}
−5	−4	−3
−3*	−2	−1
−1	0	0.7*
1	1.4*	3
3	4	5

TABLE 4. Imposed sensitivity values of a'' and N_{0S}. Only one variable is modified for each of these sensitivity cases; the other variable is set to the control value. An asterisk denotes the control setting for each cloud case.

a''	N_{0S} (m^{-4})
0.5875	5.0×10^6
1.175	1.0×10^7
2.35*	2.0×10^7*
4.70	4.0×10^7
9.40	8.0×10^7

their control values. Then we perform the simulation and calculate snow mixing ratio and flux at cloud base.

One benefit of any scaling law is that it combines the effects of several parameters into a single formula, thereby reducing scatter that would arise if the formula depended on only one of these parameters. To test how well our scaling law collapses the scatter, we first construct a benchmark with which to compare the scaling laws by plotting r_S at cloud base as computed by LES versus four individual parameters, namely, $1/a''^2$, N_{0S}, Δz^2, and $(\langle S_i \rangle - 1)^2$ (Fig. 2). We have squared some of the aforementioned parameters because the exponent for these terms in Eq. (34) is approximately 2 for spheres. Consequently, squaring each of these terms

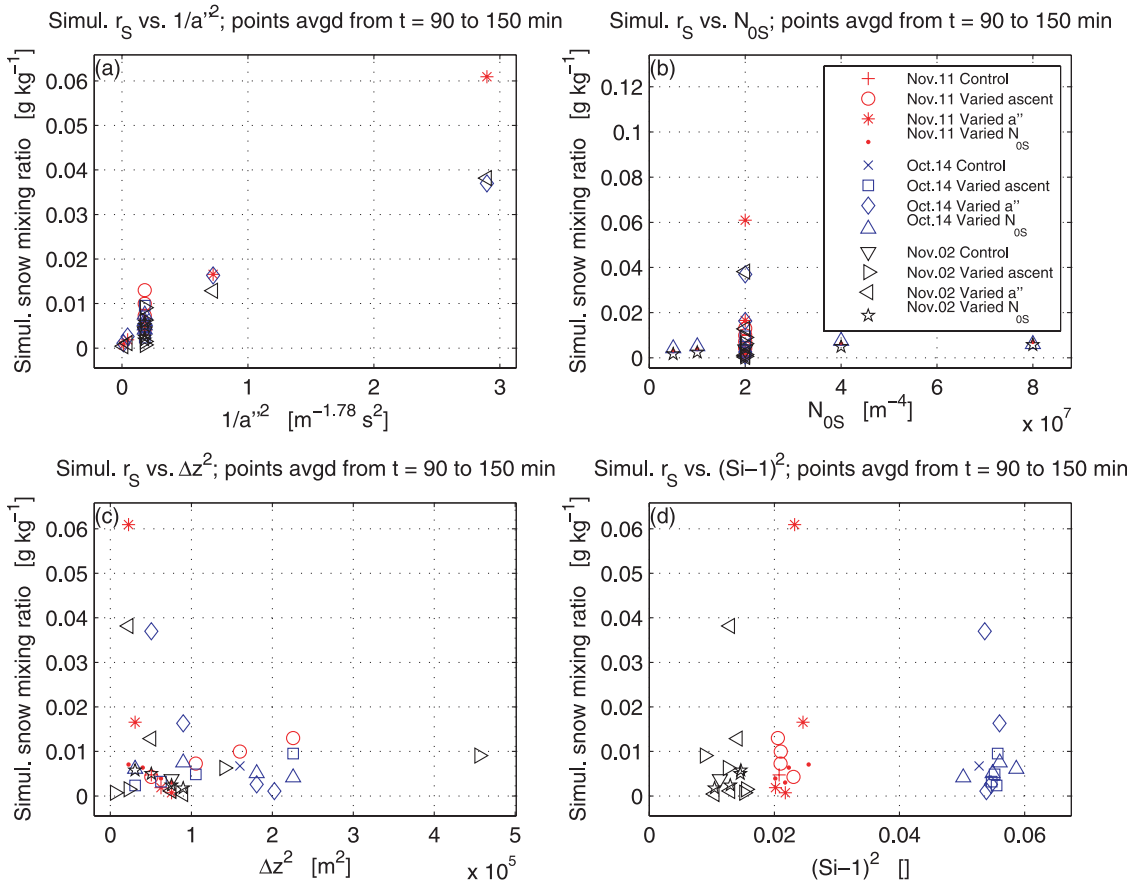

FIG. 2. Scatterplots of snow mixing ratio (r_S) at cloud base vs four variables that vary across our sensitivity simulations: (a) the dependence of r_S on the coefficient of the fall speed–diameter relationship a'' (14), (b) the snow intercept parameter N_{0S} (6), (c) the thickness of the mixed-phase layer squared, $\Delta z^2 = (z_{top} - z_{base})^2$, and (d) the supersaturation with respect to ice minus 1 ($S_i - 1$) [(21)]. Each point represents one sensitivity simulation, as labeled in the figure legend. The output is time averaged over 1 h. When the variables are varied independently, none except for a'' exhibits correlation with r_S, but even for a'' the scatter is significant.

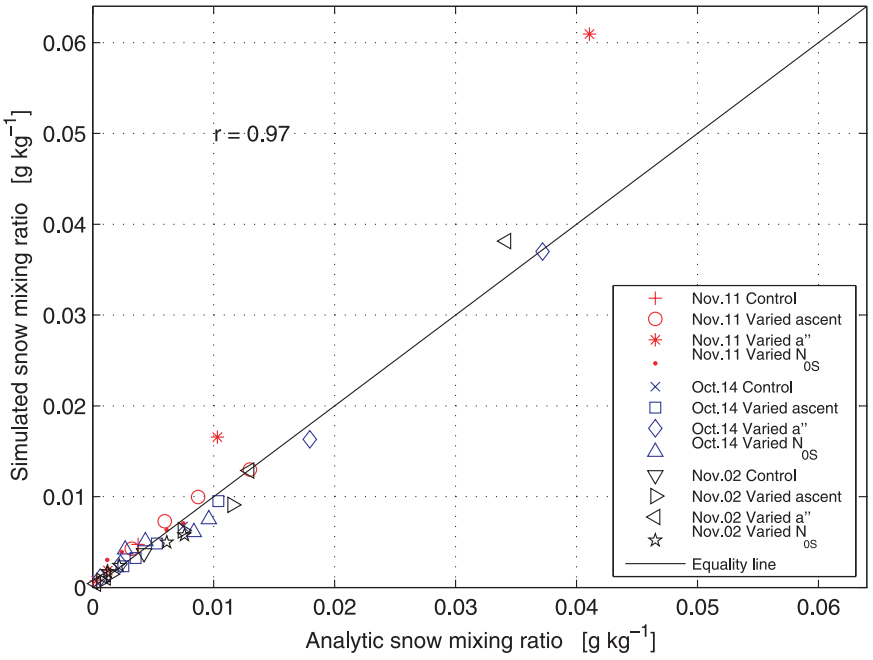

FIG. 3. A scatterplot comparing values of snow mixing ratio r_S at cloud base as estimated by our analytic Eq. (35) and the COAMPS-LES sensitivity simulations. Each point represents one sensitivity simulation, as denoted in the figure legend. The solid line indicates equality between analytic and simulated values of r_S. Points above and to the left of the line indicate an underestimate by our analytic formula; points to the right and below indicate an overestimate. The scatter is reduced as compared to Fig. 2.

should produce the best match between the LES and analytical scaling laws. Each scatter point corresponds to a 1-h average of a single sensitivity simulation. The horizontal gaps between points in Figs. 2a and 2b arise from the fact that a'' and N_{0S} are specified to have the discrete values listed in Table 4. Snow mixing ratio r_S is evidently positively correlated with $1/a''^2$, as expected from Eq. (34), but the linear scale of the plot obscures the degree of scatter. For instance, the column of points at $1/a''^2 = 0.18$ ranges by a factor of 17, from $r_S = 7 \times 10^{-4}$ to 1.2×10^{-2} g kg^{-1}. There is no discernable correlation between r_S and N_{0S}, Δz^2, or $(\langle S_i \rangle - 1)^2$. The imperfect correlation of r_S with each of the four individual parameters is unsurprising, given that all four parameters cooperate jointly to determine r_S.

If we combine the four aforementioned parameters as in the analytic scaling law (35), the scatter in Fig. 2 collapses onto a single curve (Fig. 3). The linear correlation coefficient (Press et al. 2007, p. 745) between the LES value of r_S and the analytic value of r_S as estimated by (35) is $r = 0.97$. The fit is good except for one outlier that corresponds to a low value of a'' for the 11 November case (red asterisk).

On a linear scale, it is difficult to assess the quality of the fit for small values of r_S. Therefore, we replot the same data but on a log–log scale (Fig. 4). This plot reveals that, even for low values of r_S, the analytic formula performs adequately. Furthermore, the plot shows that the range of validity of the scaling law is two orders of magnitude, with r_S spanning from 3×10^{-4} to 4×10^{-2} g kg^{-1}.

The snow mixing ratio r_S does not directly determine glaciation rate. A more direct indicator of glaciation rate is the sedimentation flux of snow from cloud base, $w_S r_S$, which is related to the net depletion of liquid by snow over the depth of the cloud [see Eq. (38) above]. Figure 5 plots analytic versus LES values of $w_S r_S$ using the same sensitivity simulations as in Figs. 3 and 4 above. The fit is still acceptable, with a linear correlation coefficient $r = 0.90$. The same data points are plotted on a log–log scale in Fig. 6. This shows that the scaling law extends over one order of magnitude. The points are more scattered than for the r_S scaling law, particularly for sensitivity simulations that change the fall speed–diameter coefficient a''.

6. Application to other platelike and dendritic habits

Our derivation of the snow mixing ratio r_S and snow flux $w_S r_S$ is valid for arbitrary positive values of

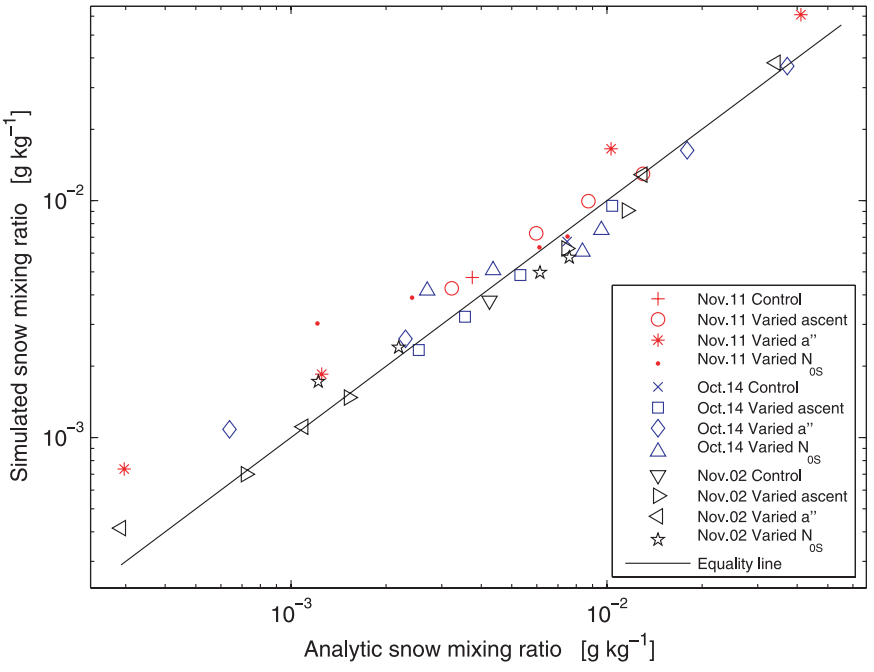

FIG. 4. A log–log plot of the same data points shown on a linear scale in Fig. 3. Unlike the linear plot, the log–log plot shows that the fit is still acceptable even for small values of r_S at cloud base and that the analytic scaling law is valid over a range of two orders of magnitude.

mass–diameter prefactor α and exponent β, and fall speed–diameter prefactor a'' and exponent b. Testing all possible combinations of parameter values using LES is computationally prohibitive. Therefore, although our sensitivity study does vary a'', we specify α, β, and b using the default values of COAMPS-LES. However, it is of interest to study other parameter values theoretically, on the assumption that the level of accuracy simulated for the tested values holds more generally.

In particular, we wish to calculate the glaciation rates associated with varying habit types, which have varying mass–diameter and fall speed–diameter coefficients. We consider various platelike and dendritic habits but do not consider needles or long columns because their capacitance is not a power-law function of diameter (Pruppacher and Klett 1997), as assumed by our derivation [see Eq. (22)]. Also, we do not consider rimed habits because our derivation does not include growth by accretion. The coefficients of the additional habits considered are obtained from Heymsfield and Kajikawa (1987) and are listed in Table 5. The habit types range from simple plates to complex polycrystals. The exponents of the mass–diameter relationships vary moderately (β = [2.02, 3.31]), and the exponents of the fall speed–diameter relationships vary somewhat more (b = [0.11, 1.09]).

We now substitute the pairs of [β, b] values listed in the rows of Table 5 into the expressions for r_S (34), w_S (36), and $w_S r_S$ (37) to find the range of their exponents. These ranges are listed in exponentiated brackets in the equation below. We assume a power-law capacitance (22) that is appropriate for a plate, $\gamma = \nu = 1$ (Rogers and Yau 1989). Furthermore, we assume hereafter that $z = z_{\text{cloud base}}$, and that, therefore, $z_{\text{top}} - z = \Delta z$, the mixed-phase cloud thickness. Then

$$
\begin{aligned}
r_S &\propto N_{0S}^{1} \\
&\propto [(\langle S_i \rangle - 1)\Delta z]^{(\beta+1)/(\beta+b-\nu)} \cong [(\langle S_i \rangle - 1)\Delta z]^{[1.3,2.5]} \\
&\sim [(\langle S_i \rangle - 1)\Delta z]^{2} \\
&\propto a''^{(-\beta-1)/(\beta+b-\nu)} \cong a''^{[-1.3,-2.5]} \sim a''^{-2} \\
&\propto \alpha^{(b-\nu-1)/(\beta+b-\nu)} \cong \alpha^{[-0.3,-1.5]} \sim \alpha^{-1}; \qquad (41)
\end{aligned}
$$

$$
\begin{aligned}
w_S &\propto N_{0S}^{0} \\
&\propto [(\langle S_i \rangle - 1)\Delta z]^{b/(\beta+b-\nu)} \cong [(\langle S_i \rangle - 1)\Delta z]^{[0.05,0.4]} \\
&\sim [(\langle S_i \rangle - 1)\Delta z]^{0} \\
&\propto a''^{(\beta-\nu)/(\beta+b-\nu)} \cong a''^{[0.6,0.95]} \sim a''^{1} \\
&\propto \alpha^{-b/(\beta+b-\nu)} \cong \alpha^{[-0.05,-0.4]} \sim \alpha^{0}; \qquad (42)
\end{aligned}
$$

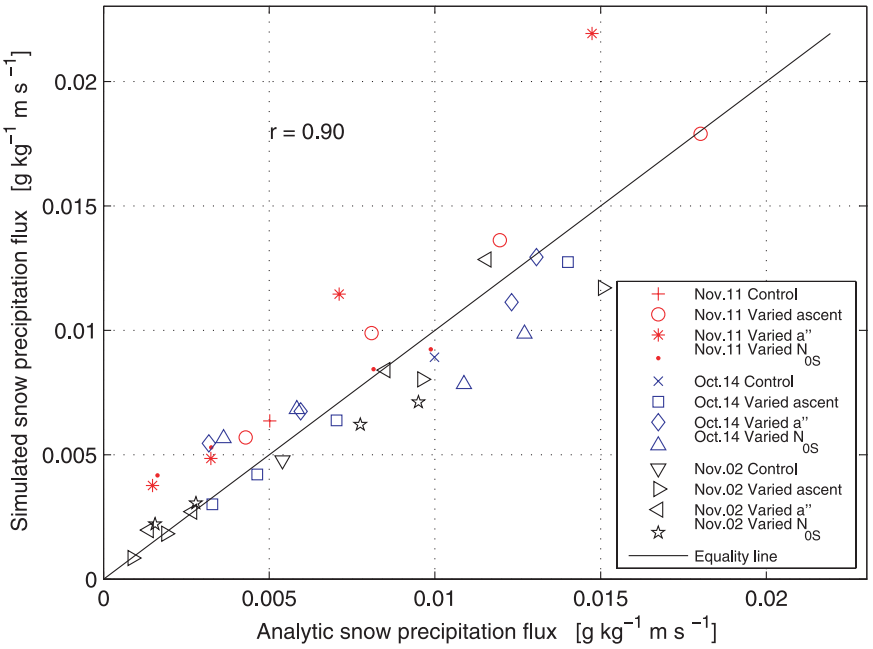

FIG. 5. As in Fig. 3 but for the flux of snow mixing ratio $w_S r_S$ at cloud base [i.e., the product of (36) and (35)]. The points are more scattered than for the r_S scaling, but nonetheless the fit is acceptable.

$$
\begin{aligned}
w_S r_S &\propto N_{0S}^1 \\
&\propto [(\langle S_i \rangle - 1)\Delta z]^{(\beta+b+1)/(\beta+b-\nu)} \cong [(\langle S_i \rangle - 1)\Delta z]^{[1.6,2.6]} \\
&\cong [(\langle S_i \rangle - 1)\Delta z]^2 \\
&\propto a''^{(-\nu-1)/(\beta+b-\nu)} \cong a''^{[-0.6,-1.6]} \sim a''^{-1} \\
&\propto \alpha^{(-\nu-1)/(\beta+b-\nu)} \cong \alpha^{[-0.6,-1.6]} \sim \alpha^{-1}. \qquad (43)
\end{aligned}
$$

The ranges of exponents in brackets stem from the range of $[\beta, b]$ values in Table 5. The integer exponents, listed last in each row, are the medians of the ranges of each exponent, rounded to the nearest integer. The same values of the exponents would also be obtained if we set $\beta = 3$, $b = 0$, and $\nu = 1$. Note that the integer exponents on $w_S r_S$ are simply the sums of the corresponding exponents on w_S and r_S.

We interpret some of these scaling exponents as follows:

1) We see that $w_S \propto N_{0S}^0$ and that r_S and $w_S r_S$ are proportional to N_{0S}^1. The fact that $w_S \propto N_{0S}^0$ is unsurprising because adding more snow crystals would not be expected to change the fall speed of individual crystals, all else being equal (i.e., all other explicit parameters—such as S_i, Δz, etc.—being held fixed). Similarly, r_S and $w_S r_S$ are proportional to N_{0S}^1 because doubling the number of snow crystals would be expected to double r_S and $w_S r_S$, if all else remains equal.
2) Both r_S and $w_S r_S$ increase strongly with increasing $[(\langle S_i \rangle - 1)\Delta z]$. This is because a moister, thicker layer enhances depositional growth of snow.

More specifically, in the expression (41) for r_S, the exponent of $[(\langle S_i \rangle - 1)\Delta z]$, namely $(\beta + 1)/(\beta + b - \nu)$, may be interpreted as follows. Combining Eq. (13) ($r_S \propto N_S \overline{D_S}^{\beta}$) and Eq. (12) ($N_S = N_{0S}\overline{D_S}$), we find $r_S \propto D_S^{(\beta+1)}$. The extra 1 in the exponent arises from the assumption that N_S increases linearly with $\overline{D_S}$. Combining this with our previous finding that $\overline{D_S} \propto [(\langle S_i \rangle - 1)\Delta z]^{[1/(\beta+b-\nu)]}$ [Eq. (32)], we obtain $\overline{r_S} \propto [(\langle S_i \rangle - 1)\Delta z]^{[(\beta+1)/(\beta+b-\nu)]}$ [Eq. (41)].

The fact that r_S and $w_S r_S$ are roughly proportional to $[(\langle S_i \rangle - 1)\Delta z]^2$ rather than to $[(\langle S_i \rangle - 1)\Delta z]^1$ is perhaps surprising. The reason for the enhanced dependence is that, as the snow crystals fall, they are assumed to become more numerous, and their increased surface area increases the rate of deposition on them. The relationship $w_S r_S \propto [(\langle S_i \rangle - 1)\Delta z]^1$ would occur if the mean number concentration N_S and capacitance C were constant [see Eq. (33)]. In contrast, we follow RH83 in choosing $N_S \propto \overline{D_S}$ (12) and $C \propto \overline{D_S}^{\nu} = \overline{D_S}^1$ (22). Both of these factors contribute to the exponent value of 2. The fact that $N_S \propto \overline{D_S}$ is assumed increases the exponent on r_S because $r_S \propto N_S \overline{D_S}^{\beta}$. That is, as $\overline{D_S}$ grows in size,

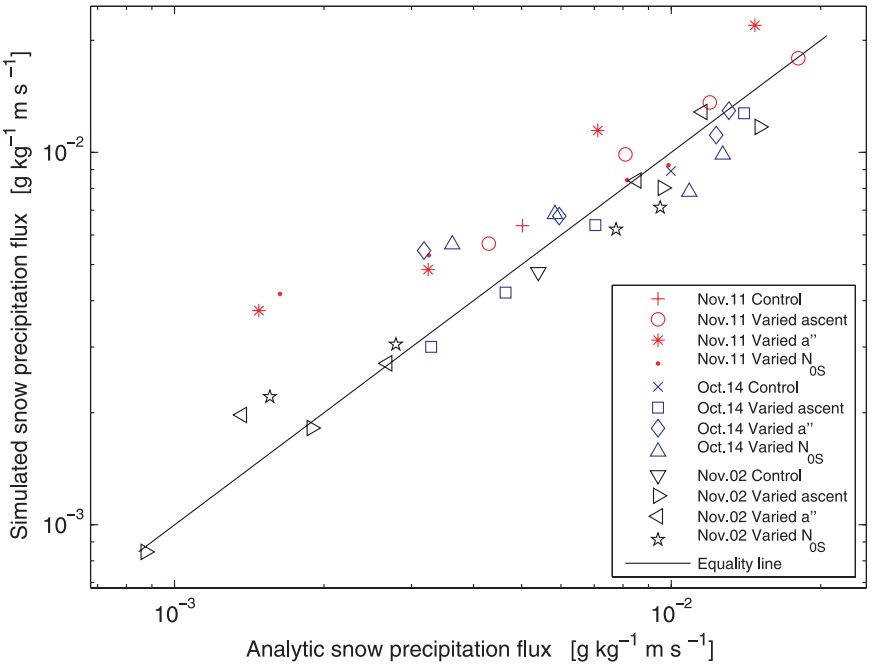

FIG. 6. A log–log plot of the same data points shown on a linear scale in Fig. 5. The log–log plot shows that the fit is acceptable even for points with small snow flux and that the scaling extends for one order of magnitude in snow flux.

N_S increases in number, leading to greater r_S. The fact that $C \propto D_S^1$ causes a positive feedback. If D_S increases, so does C. But recall that C can be interpreted as a coefficient that increases the depositional growth rate for a given value of S_i [see Eq. (21)]. Therefore, if C increases, so does $\overline{D_S}$, thereby completing the positive feedback that ultimately increases r_S.

3) The fall speed w_S increases with increasing a'' because of the linear relationship between the two for fixed $\overline{D_S}$ [see Eq. (18)] and because $b \lesssim \beta - \nu$, which implies that r_S tends to adjust more to a change in a parameter such as a'' than does w_S [see Eq. (33)].
4) In contrast, r_S decreases strongly with increasing a''. If a'' increases, w_S increases. Then the snow crystal falls faster, spends less time in cloud, and grows less, leading to smaller r_S. Mathematically, $r_S \propto \overline{D_S}^{\beta+1}$ (13) and $\overline{D_S} \propto a''^{-1/(\beta+b-\nu)}$ (32).
5) Equation (41) shows that r_S decreases with increasing α. This is less intuitive, given that r_S increases

TABLE 5. Mass–diameter coefficient (α) and exponent (β) [defined in Eq. (8)], and the fall speed–diameter coefficient (a'') and exponent (b) [defined in Eq. (14)]. Values are obtained from Heymsfield and Kajikawa (1987) and are used for the snow crystal habits plotted in Fig. 7. The first row lists default values used in the COAMPS-LES model.

Habit designation	Habit description	α	β	a''	b	Oct 14 $w_S r_S$ (m s^{-1} kg kg^{-1})
COAMPS		1	3	2.35	0.11	0.010
C1h	Thick plate	0.12	2.68	2205	1.09	0.012
P1a	Hexagonal plate	3.0	3.31	156	0.86	0.054
P1b	Plate with sectorlike branches	0.055	2.83	79	0.81	0.12
P1c	Plate with broad branches	0.027	2.79	18	0.62	0.23
P1d	Stellar crystal	0.0028	2.59	7.3	0.55	0.91
P1e	Dendrite	0.000 44	2.29	5.0	0.48	1.1
P2a	Stellar with end plates	0.0046	2.53	3.3	0.33	0.23
P2c	Dendrite with end plates	0.088	3.12	1.4	0.20	0.46
P2e	Plate with simple extensions	0.034	2.81	29.6	0.68	0.19
P6c	Stellar with spatial plates	0.000 13	2.02	1.5	0.21	0.37
P6d	Stellar with spatial dendrites	0.0022	2.55	3.3	0.37	0.74
P7b	Radiating assemblage of dendrites	0.0067	2.68	62.6	0.83	0.41

with increasing α if $\overline{D_S}$ is held fixed [see Eq. (13)]. Large α implies that crystals are "dense"—that is, that even small-diameter crystals have large mass, according to the mass–diameter relationship (8). The reason for the opposite dependence, namely that r_S decreases if α increases, is that $\overline{D_S}$ decreases if α increases, as can be seen from (32) or (33), and r_S depends strongly on $\overline{D_S}$ [see Eq. (13)]. Mathematically, $r_S \propto \alpha \overline{D_S}^{\beta+1}$ (13) and $\overline{D_S} \propto \alpha^{-1/(\beta+b-\nu)}$ (32). An alternative interpretation is that, when α is large, the snow crystals are dense and therefore fall rapidly, leaving less time for growth and leading to smaller r_S [see Eqs. (19) and (42)].

6) The fall speed w_S varies weakly with $[(\langle S_i \rangle - 1)\Delta z]$ and α.

To summarize the preceding comments, Fig. 7 displays a plot of the relationship between habit type and the exponents of r_S and $w_S r_S$. The exponents relate r_S and $w_S r_S$ to $[(\langle S_i \rangle - 1)\Delta z]$, a'', and α. In Fig. 7, we set $\nu = 1$, contour the exponents as a function of β and b, and overplot the corresponding exponent values from the various habit types. The correlation between habit type and exponent is imperfect but, overall, the simpler platelike shapes (e.g., C1h and P1a) have exponents of smaller magnitude, both positive and negative, and the more complex dendritic forms (e.g., P1e, P2c, and P6d) have exponents of larger magnitude (see Table 5). This implies, for instance, that r_S increases more rapidly with increasing S_i for dendrites than for plates. In other words, if S_i is larger in one cloud than in another, then the ratio of r_S in the large-S_i cloud to the small-S_i cloud is larger for dendrites than plates, all else being equal.

The exponents, however, do not tell the full story. Although the exponents vary in magnitude, larger variations occur in the *prefactors* for the mass–diameter ($\alpha = [0.00013, 3.0]$) and fall speed–diameter ($a'' = [1.4, 2205]$) relationships (see Table 5). Furthermore, the exponents β and b enter Eqs. (34) and (37) in ways other than as exponents to $[(\langle S_i \rangle - 1)\Delta z]$, a'', or α. The complex interplay between prefactors and exponents makes it difficult to understand the relationship between particular parameter values and the magnitudes of r_S and $w_S r_S$. Nevertheless, the final column of Table 5 suggests that more complex or dendritic habits tend to produce larger values of $w_S r_S$ at cloud base. Presumably, this is because dendrites have a larger surface to mass ratio, leading to (i) a slower fall speed and a larger residence time in cloud and (ii) a more rapid depositional growth rate [see Eq. (5)].

7. Discussion and conclusions

This paper has derived a scaling law for the sedimentation flux of snow out of cloud base, $w_S r_S$ (37). The quantity $w_S r_S$ is related to the within-cloud depositional growth of snow [see Eq. (38)], which is in turn related by the Wegener–Bergeron–Findeisen process to depletion of liquid. Therefore, the scaling law has relevance to the glaciation rate of mixed-phase clouds. In fact, it is closely related to a glaciation time scale, τ_G (40). We also derive individual scaling laws for snow mixing ratio r_S (34) and crystal fall speed w_S (36). All of these are derived from an equation for depositional growth of snow (1). We do not believe that the best use of the scaling laws is as a parameterization in a large-scale host model since large-scale host models can simply integrate the depositional growth equation directly and thereby avoid approximation. Rather, we believe that the greater use of the scaling laws is conceptual.

The scaling laws rely on numerous assumptions based on a single-moment microphysical framework. They neglect aggregation, accretion, and turbulent transport of snow. They assume that the snow persists in a statistically steady state. Our tests of the scaling laws have limitations as well—namely, we compare the scaling laws to sensitivity simulations based on just three thin altostratocumulus clouds that cover a limited range of conditions.

Despite these caveats, in our limited tests the scaling law for snow mixing ratio holds over two orders of magnitude with a linear correlation coefficient of $r = 0.97$, and the scaling law for snow flux holds over one order of magnitude with $r = 0.90$. This demonstrates that the scaling laws capture the rudiments of depositional snow growth in thin mixed-phase layer clouds as modeled in COAMPS-LES.

How would our results have changed if we had held constant the number concentration of snow, N_S, instead of letting $N_S \propto \overline{D_S}$? Retracing the derivation, we find that to handle this case, the exponents on the scalings for r_S (41), w_S (42), and $w_S r_S$ (43) must undergo the transformation

$$\begin{aligned} \beta &\rightarrow \beta - 1 \\ \nu &\rightarrow \nu - 1, \quad \text{where} \\ N_{0S} &\rightarrow N_S. \end{aligned} \tag{44}$$

This leads to exponents of smaller magnitude for r_S and $w_S r_S$ but leaves the exponent for w_S unchanged.

The derivation of our formulas for r_S (34), w_S (36), and $w_S r_S$ (37) allow arbitrary positive values of the coefficients α, β, a'', and b. Therefore, the formula can calculate the glaciation rates of different habit types. We explore two classes of habits, platelike and dendritic, and obtain quantitative values of exponents for r_S (41), w_S (42), and $w_S r_S$ (43). We find that dendritic

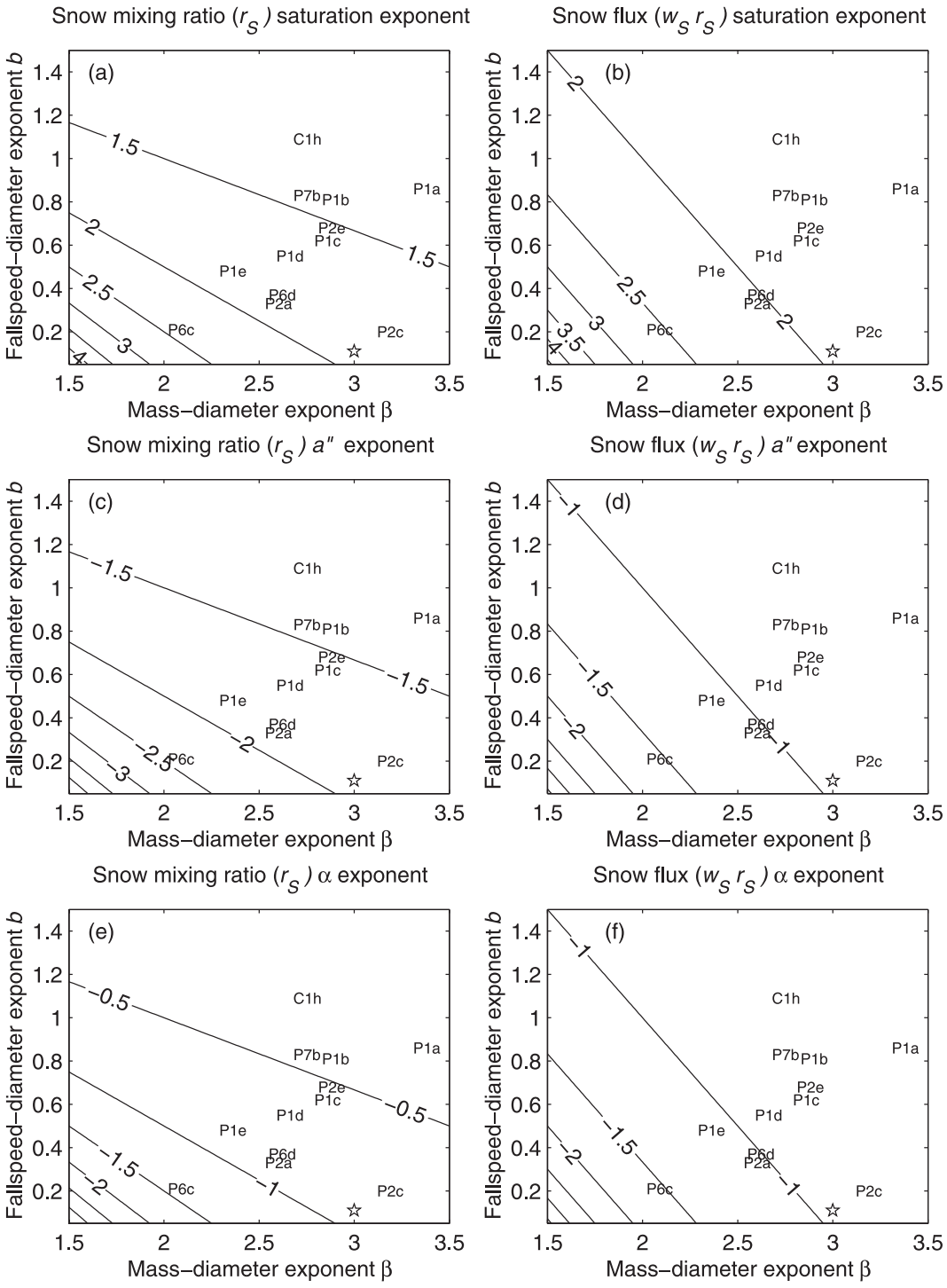

FIG. 7. Contour plots of the values of the exponents of (top) $(\langle S_i \rangle - 1)$ $(z_{\text{top}} - z)$, (middle) a'', and (bottom) α in the equations for (left) r_S (34) and (right) $w_S r_S$ (37). The x axis is the mass–diameter exponent β (8); the y axis is the fall speed–diameter exponent b (14). In both panels, we assume that the crystal capacitance exponent ν equals 1. The star indicates the values of (β, b) used in the COAMPS-LES model. The alphanumeric labels locate the exponents (Heymsfield and Kajikawa 1987) of other platelike habit types (Magono and Lee 1966). More complex, dendritic habits tend to have exponents with higher magnitudes than do simpler platelike habits.

habits tend to increase their glaciation rate more rapidly than platelike habits when the layer becomes moister and thicker (see Table 5). However, the reasons for this are complex and cannot be attributed to a single factor.

We hope that the scaling laws described here will aid understanding of the evolution of liquid and snow in mixed-phase layer clouds in a variety of geographic locations and with a variety of snow habit types. Although focused on the application of the scaling laws to midlevel midlatitude clouds, we believe that the scaling laws may also apply to some thin, mixed-phase Arctic clouds, whether at midlevels or in the boundary layer.

Acknowledgments. We thank three anonymous referees for their reviews of this manuscript. V. E. Larson and A. J. Smith are grateful for financial support provided by the UWM Research Growth Initiative and by Grant ATM-0618818 from the National Science Foundation. COAMPS is a registered trademark of the Naval Research Laboratory.

REFERENCES

Ackerman, T. P., and Coauthors, 2004: Atmospheric Radiation Measurement program science plan. U.S. Department of Energy Rep. DOE/ER-ARM-0402, 62 pp. [Available online at http://www.arm.gov/publications/programdocs/doe-er-arm-0402.pdf.]

Bergeron, T., 1935: On the physics of clouds and precipitation. *Proces Verbaux de l'Association de Météorologie,* Lisbon, Portugal, International Union of Geodesy and Geophysics, 156–178.

Bragg, M. B., W. R. Perkins, N. B. Sarter, T. Basar, P. G. Voulgaris, H. M. Gurbacki, J. W. Melody, and S. A. McCray, 1998: An interdisciplinary approach to inflight aircraft icing safety. *Proc. 36th Aerospace Sciences Meeting and Exhibit,* Reno, NV, American Institute of Aeronautics and Astronautics, AIAA-2000-0360.

Carey, L. D., J. Niu, P. Yang, J. A. Kankiewicz, V. E. Larson, and T. H. Vonder Haar, 2008: The vertical profile of liquid and ice water content in midlatitude mixed-phase altocumulus clouds. *J. Appl. Meteor. Climatol.,* **47,** 2487–2495.

Cober, S. G., G. A. Isaac, and J. W. Strapp, 2001: Characterizations of aircraft icing environments that include supercooled large drops. *J. Appl. Meteor.,* **40,** 1984–2002.

Cooper, W. A., 1986: Ice initiation in natural clouds. *Precipitation Enhancement—A Scientific Challenge, Meteor. Monogr.,* No. 43, Amer. Meteor. Soc., 29–32.

Duynkerke, P. G., and Coauthors, 2004: Observations and numerical simulations of the diurnal cycle of the EUROCS stratocumulus case. *Quart. J. Roy. Meteor. Soc.,* **130,** 3269–3296.

Falk, M. J., and V. E. Larson, 2007: What causes partial cloudiness to form in multilayered midlevel clouds? A simulated case study. *J. Geophys. Res.,* **112,** D12206, doi:10.1029/2006JD007666.

Findeisen, W., 1938: Kolloid-meteorologische vorgänge bei Neiderschlags-Bildung. *Meteor. Z.,* **55,** 121–133.

Fleishauer, R. P., V. E. Larson, and T. H. Vonder Haar, 2002: Observed microphysical structure of midlevel, mixed-phase clouds. *J. Atmos. Sci.,* **59,** 1779–1804.

Fletcher, N. H., 1962: *The Physics of Rainclouds*. Cambridge University Press, 386 pp.

Golaz, J.-C., S. Wang, J. D. Doyle, and J. M. Schmidt, 2005: Second- and third-moment vertical velocity budgets derived from COAMPS-LES. *Bound.-Layer Meteor.,* **116,** 487–517.

Harrington, J. Y., T. Reisin, W. R. Cotton, and S. M. Kreidenweis, 1999: Cloud-resolving simulations of Arctic stratus. Part II: Transition-season clouds. *Atmos. Res.,* **51,** 45–75.

Haulman, D. L., 2003: U.S. unmanned aerial vehicles in combat, 1991–2003. Air Force Historical Research Agency Rep., 19 pp.

Heymsfield, A. J., and M. Kajikawa, 1987: An improved approach to calculating terminal velocities of plate-like crystals and graupel. *J. Atmos. Sci.,* **44,** 1088–1099.

Hobbs, P. V., and A. L. Rangno, 1985: Ice particle concentrations in clouds. *J. Atmos. Sci.,* **42,** 2523–2549.

Hodur, R. M., 1997: The Naval Research Laboratory's Coupled Ocean/Atmosphere Mesoscale Prediction System (COAMPS). *Mon. Wea. Rev.,* **125,** 1414–1430.

Kankiewicz, J. A., L. D. Carey, J. M. Davis, J. M. Forsythe, D. L. Reinke, and T. H. Vonder Haar, 2002: The morphology of two mixed phase clouds. Preprints, *11th Conf. on Cloud Physics,* Ogden, UT, Amer. Meteor. Soc., 6.1. [Available online at http://ams.confex.com/ams/pdfpapers/42113.pdf.]

Korolev, A. V., and P. R. Field, 2008: The effect of dynamics on mixed-phase clouds: Theoretical considerations. *J. Atmos. Sci.,* **65,** 66–86.

Larson, V. E., R. P. Fleishauer, J. A. Kankiewicz, D. L. Reinke, and T. H. Vonder Haar, 2001: The death of an altocumulus cloud. *Geophys. Res. Lett.,* **28,** 2609–2612.

——, A. J. Smith, M. J. Falk, K. E. Kotenberg, and J.-C. Golaz, 2006: What determines altocumulus dissipation time? *J. Geophys. Res.,* **111,** D19207, doi:10.1029/2005JD007002.

——, K. E. Kotenberg, and N. B. Wood, 2007: An analytic longwave radiation formula for liquid layer clouds. *Mon. Wea. Rev.,* **135,** 689–699.

Liou, K. N., 2002: *An Introduction to Atmospheric Radiation*. 2nd ed. Academic Press, 583 pp.

Long, M. L., 2003: COAMPS version 3 model description—General theory and equations. Naval Research Laboratory Publication NRL/PU/7500-03-448, 143 pp.

Magono, C., and C. W. Lee, 1966: Meteorological classification of natural snow crystals. *J. Fac. Sci. Hokkaido Univ.,* **7,** 321–335.

Marsham, J. H., S. Dobbie, and R. J. Hogan, 2006: Evaluation of a large-eddy model simulation of a mixed-phase altocumulus cloud using microwave radiometer, lidar, and Doppler radar data. *Quart. J. Roy. Meteor. Soc.,* **132,** 1693–1715.

Meyers, M. P., P. J. De Mott, and W. R. Cotton, 1992: New primary ice-nucleation parameterizations in an explicit cloud model. *J. Appl. Meteor.,* **31,** 708–721.

Morrison, H., M. D. Shupe, J. O. Pinto, and J. A. Curry, 2005: Possible roles of ice nucleation mode and ice nuclei depletion in the extended lifetime of Arctic mixed-phase clouds. *Geophys. Res. Lett.,* **32,** L18801, doi:10.1029/2005GL023614.

Niu, J., L. D. Carey, P. Yang, and T. H. Vonder Haar, 2008: Optical properties of a vertically inhomogeneous mid-latitude mid-level mixed-phase altocumulus in the infrared region. *Atmos. Res.,* **88,** 234–242.

Pinto, J. O., 1998: Autumnal mixed-phase cloudy boundary layers in the Arctic. *J. Atmos. Sci.,* **55,** 2016–2038.

Press, W. H., S. A. Teukolsky, W. T. Vetterling, and B. P. Flannery, 2007: *Numerical Recipes: The Art of Scientific Computing*. 3rd ed. Cambridge University Press, 1235 pp.

Pruppacher, H. R., and J. D. Klett, 1997: *Microphysics of Clouds and Precipitation*. 2nd ed. Kluwer Academic, 954 pp.

Rauber, R. M., and A. Tokay, 1991: An explanation for the existence of supercooled water at the top of cold clouds. *J. Atmos. Sci.,* **48,** 1005–1023.

Rogers, R. R., and M. K. Yau, 1989: *A Short Course in Cloud Physics*. 3rd ed. Butterworth-Heinemann, 290 pp.

Rutledge, S. A., and P. V. Hobbs, 1983: The mesoscale and microscale structure of organization of clouds and precipitation in midlatitude cyclones. VIII: A model for the ''seeder–feeder'' process in warm-frontal rainbands. *J. Atmos. Sci.,* **40,** 1185–1206.

Shettle, E. P., and J. A. Weinman, 1970: The transfer of solar irradiance through inhomogeneous turbid atmospheres evaluated by Eddington's approximation. *J. Atmos. Sci.,* **27,** 1048–1055.

Smith, A. J., V. E. Larson, J. Niu, J. A. Kankiewicz, and L. D. Carey, 2009: Processes that generate and deplete liquid water and snow in thin midlevel, mixed-phase clouds. *J. Geophys. Res.,* **114,** D12203, doi:10.1029/2008JD011531.

Stevens, B., and Coauthors, 2005: Evaluation of large-eddy simulations via observations of nocturnal marine stratocumulus. *Mon. Wea. Rev.,* **133,** 1443–1462.

Sun, Z., and K. P. Shine, 1994: Studies of the radiative properties of ice and mixed-phase clouds. *Quart. J. Roy. Meteor. Soc.,* **120,** 111–137.

Wegener, A., 1911: *Thermodynamik der Atmosphäre*. J. A. Barth Verlag, 311 pp.